Ab initio thermodynamic study of the structure and chemical bonding of a β-$Ni_{1-x}Al_x$/α-Al_2O_3 interface

Hongtao Li,[1,2] Jiwei Feng,[1] Wenqing Zhang,[1,*] Wan Jiang,[1] Hui Gu,[1] and John R. Smith[3]
[1]*State Key Laboratory of High Performance Ceramics and Superfine Microstructures, Shanghai Institute of Ceramics, Chinese Academy of Sciences, Shanghai 200050, China*
[2]*Graduate University of Chinese Academy of Sciences, Beijing 100049, China*
[3]*Department of Materials Science and Engineering, University of Michigan, Ann Arbor, Michigan 48109, USA*
(Received 11 June 2009; revised manuscript received 14 October 2009; published 23 November 2009)

The properties of an interface between a metallic *alloy* and an *oxide* are computed by combining *ab initio* quantum mechanics with thermodynamics. Results for the stability, structures, and chemical compositions of the β-$Ni_{1-x}Al_x$/α-Al_2O_3 interface are presented. We found that there are two types of stable structures for the interface. Type I is characterized by joining an Al-rich Ni-Al alloy with an Al-rich Al_2O_3 surface (terminated by two Al atomic layers). Type II is a junction of a Ni-rich Ni-Al alloy with an Al_2O_3 surface terminated by an oxygen atomic layer and with atomic migrations and interchanges within the interfacial region. Both types of interfaces exhibit Al accumulation on top of the oxide scale while an adjacent Ni-rich layer is found at the type-II interfaces. The atomic geometries, electronic structures, and chemical bonds of the two types of interfacial systems were analyzed. The calculated interfacial works of separation W_{sep} agree reasonably well with experimental data and earlier calculations.

DOI: 10.1103/PhysRevB.80.205422 PACS number(s): 68.35.Np, 82.65.+r

I. INTRODUCTION

The adhesion of metal/ceramic interfaces[1–3] is well known to be important in industry for such applications as electronic packaging, heterogeneous catalysis, and high-temperature composite materials. The high-temperature structural intermetallic compound Ni-Al (Ref. 4) has been widely applied as a bond coat on gas turbine components in order to provide a thermally grown Al_2O_3 layer between the bond coat and the ZrO_2-based thermal barrier coatings (TBC).[5] The Al_2O_3 layer acts as an oxygen diffusion barrier, inhibiting oxidation of the Ni-Al superalloy, and thus stabilizing the performance of the whole TBC system. As is well known, the failure of those Ni-Al-based integrated TBC systems stems from the spallation of the substrate/Al_2O_3 interface, i.e., the β-$Ni_{1-x}Al_x$/α-Al_2O_3 interface. A considerable number of studies[6–16] focused on oxidation and corrosion protection of the Ni-Al alloy, the structures of the ultrathin Al_2O_3 scale on the Ni-Al substrate, and the interfacial microstructures between the Ni-Al-based alloy and the Al_2O_3. However, experimental investigations of Ni-Al alloys and related interfaces often fail to provide definitive answers to many issues,[14–17] owing to the fact that even a slight deviation from stoichiometry may affect the defect structures in Ni-Al alloys,[17] which can in turn change the structure of the interfaces. Using advanced x-ray diffraction analysis, Stierle *et al.*[14,15] claimed the existence of Al antisite atoms at the Al_2O_3/NiAl-*alloy* interface. However, Kresse *et al.*[16] inferred the opposite conclusion, i.e., that no Ni or Al antisite atoms were observed at a similar interface. Here we provide a systematic and fundamental theoretical study combining *ab initio* quantum-mechanical calculations with thermodynamics to disclose the microstructure of the β-$Ni_{1-x}Al_x$/α-Al_2O_3 interface.

A*b initio* thermodynamic methods[18,19] have been considered to be an important strategy for structure stability analyses of complex interfaces. In this approach, the Gibbs energy G_s of an ensemble such as an interface system can be expressed as

$$G_s = G_{total} - \sum_i N_i \mu_i. \quad (1)$$

Here G_{total} is the free energy of the ensemble that may contain various structures such as a surface or an interface. μ_i $(i=1,2,3,\ldots)$ are the chemical potentials of the constituents i and N_i are the corresponding numbers of atom i in the ensemble. Links can be established between variables of *ab initio* calculations and standard thermodynamic variables such as the partial pressure, activity, and chemical potential.[18] In recent years, the desire to improve advanced materials for various technological applications has stimulated considerable *ab initio* thermodynamic researches. For example, Wang *et al.*[20] computed the environmental dependence of α-Al_2O_3 (0001) surface structures. Zhang *et al.* and Finnis *et al.* studied the dependence of the stable Nb/Al_2O_3 interfacial structure on oxygen partial pressure[19,21] and the initial stages of oxidation of the Ni-Al (110) surfaces.[22]

In this paper, the *ab initio* thermodynamic method is employed to investigate the structural stability of the β-$Ni_{1-x}Al_x$/α-Al_2O_3 interface ($x \sim 0.5$), as well as its dependence on alloy composition x and oxygen partial pressure p_{O_2} at a given temperature. Results of interfacial energies, atomic relaxations, electron-density distributions, and works of separation based on a supercell approach to the β-$Ni_{1-x}Al_x$/α-Al_2O_3 interface are presented.

II. BASIC RELATIONSHIPS

To express a few basic relationships in a general way, we start from a model interface formed between a binary alloy $A_{1-x}B_x$ and an oxide phase BO_y. This type of interface could

be easily obtained through the oxidation of $Ni_{1-x}Al_x$, given that the element Al is more active than Ni. It is well known that the most stable interfacial structure has the lowest interfacial energy. To search for stable interfacial structures, the following equation is applied to estimate the interfacial energy γ_I:

$$\gamma_I = [G_{total}(T,p) - N_A\mu_A - N_B\mu_B - N_O\mu_O]/S$$
$$= \frac{1}{S}\left[G_{total} - \frac{1}{1-x}N_A\mu_{A_{1-x}B_x} - \frac{1}{y}N_O\mu_{BO_y} - \left(N_B - \frac{x}{1-x}N_A - \frac{1}{y}N_O\right)\mu_B \right]. \quad (2)$$

Thermodynamic equilibrium has been reasonably assumed between the interface and the surrounding bulk $A_{1-x}B_x$ and BO_y having the chemical potentials $\mu_{A_{1-x}B_x}$ and μ_{BO_y}, respectively. In other words, equations $(1-x)\mu_A + x\mu_B = \mu_{A_{1-x}B_x}$ and $\mu_B + y\mu_O = \mu_{BO_y}$ have been applied in the derivation of Eq. (2). N_A, N_B, and N_O are the number of the elements A, B, and O (oxygen) in the interface ensemble, and the μ_A, μ_B, and μ_O are the corresponding chemical potentials in the system that is in equilibrium with surrounding environment. G_{total} is the total free energy of the representative interfacial layers, which have a cross-sectional area S. Based on the Gibbs phase rule, there exists only one free variable, either the oxygen partial pressure p_{O_2} or the elemental activity a_B at a given temperature, which determines μ_B in Eq. (2) and the interfacial energy γ_I. For the β-$Ni_{1-x}Al_x$/α-Al_2O_3 interface, γ_I can be expressed as

$$\gamma_I = \left\{ G_{total} - \frac{N_{Ni}}{1-x}\mu_{Ni_{1-x}Al_x} - \frac{N_O}{3}\mu_{Al_2O_3} - \left(N_{Al} - \frac{2N_O}{3} - N_{Ni}\frac{x}{1-x}\right)[\Delta\mu_{Al} + \mu^0_{Al}(0\ \mathrm{K})] \right\}/S \quad (3)$$

in which $\mu^0_{Al}(0\ \mathrm{K})$ is the total energy per Al atom in the bulk fcc state at 0 K, and the effective chemical-potential difference $\Delta\mu_{Al} = \mu_{Al} - \mu^0_{Al}(0\ \mathrm{K})$ can be used to describe the environmental dependence of interface stability.[18,19,21] The relationship to the oxygen partial pressure as well as to the Al activity or Al composition in β-$Ni_{1-x}Al_x$ alloy can also be built through expressing $\Delta\mu_{Al}$ in terms of other thermodynamic variables, which will be discussed in the following sections. Furthermore, in order to avoid the divergence of the calculated interface energies due to slab model used and the error in the calculated bulk energies of Al_2O_3 and Ni-Al,[23–25] we calculate the total energies of the relaxed Al_2O_3 and Ni-Al slabs of different layers (4, 6, 8, 10, and 12 layers for Al_2O_3 and 5, 7, 9, and 11 layers for Ni-Al slabs), and then adopt a fitting procedure[23–25] to determine the total energies of bulk Al_2O_3 and Ni-Al, that is,

Total energy of a slab
= (layer number) * (energy of bulk formula)
+ 2 * (energy from surface).

In addition, large supercells of Al_2O_3 (0001) $(3\times\sqrt{3})$ and Ni-Al (110) (5×2) cells, similar to the cells in the interface model, are used for the above calculations, which are also helpful to get reliable bulk energies for interface calculations.

III. *AB INITIO* THERMODYNAMIC METHODS

A. Computational details

The density-functional plane-wave method, as implemented in the Vienna *ab initio* simulation package (VASP),[26,27] is utilized in this study. The ultrasoft pseudopotentials[28,29] are used for the expansion of the single-particle Kohn-Sham wave functions. Exchange-correlation potentials are treated with the generalized gradient approximation.[30] To ensure the convergence of results, a plane-wave cutoff energy of 400 eV and an energy convergence criterion of 10^{-4} eV for self-consistency are adopted throughout all the calculations.

Test calculations are performed for the surface and bulk properties of β-NiAl and α-Al_2O_3 at first to assess the accuracy of the pseudopotentials used for interface systems. The equilibrium lattice constants are obtained to be 2.89 Å for β-NiAl and 4.77 Å for α-Al_2O_3. The surface energies are obtained to be 1.63 $\mathrm{J/m^2}$ for Ni-Al (110) and 1.69 $\mathrm{J/m^2}$ for stoichiometric Al_2O_3 (0001) by following the fitting method as recommended in Refs. 23–25 (see the detail in Sec. II). The good convergence of surface energies shows that using four layers has been sufficient for Al_2O_3 while five layers for Ni-Al. We also test the convergence of interface energy for a stoichiometric interface, the change in interface energies is $\sim$0.01 $\mathrm{J/m^2}$ when the Al_2O_3 layers is increased to six for the stoichiometric interface. All our calculated values agree well with previous *ab initio* computations and experimental data.[4,21,22,31–34] The structure relaxations for the Al_2O_3 surface in our work also agree well with those using VASP-projector-augmented-wave (PAW)-Perdew-Burke-Ernzerhof (PBE) calculations on Fe/Al_2O_3.[33]

For interface calculations, because the interface supercell (see below) contains more than 220 atoms with a dimension as large as 14.29 Å × 8.25 Å × 29.95 Å, only a single Γ point is used for the integrals over the Brillouin zone to save computational time. Convergence tests using $2\times2\times1$ k points are carried out to compare with the results using only the Γ point. The total-energy difference is $\sim$1 meV/atom but the surface/interface energy difference is $\sim10^{-2}$ $\mathrm{J/m^2}$ for the $(Al_2O_3)_{Al}$ surface and the Al_2-terminated Al_2O_3/$Ni_{1-x}Al_x$-alloy interface. Here the subscript Al refers to a surface terminated by a single Al atomic layer, and Al_2 terminated means a surface terminated by two Al atomic layers. Calculations using $3\times3\times1$ and $4\times4\times1$ k points have also been carried out for the $(Al_2O_3)_{Al}$ surface and the Al_2-terminated interface with the large supercell approach, and the change in the total energy was found to be less than 0.5 meV for the whole supercell in comparison with the result using $2\times2\times1$ k points. Those tests imply that the Γ-point calculations are sufficiently reliable for our purposes.

The ions are relaxed toward equilibrium until the Hellmann-Feynman forces are less than 5×10^{-2} eV/Å. For

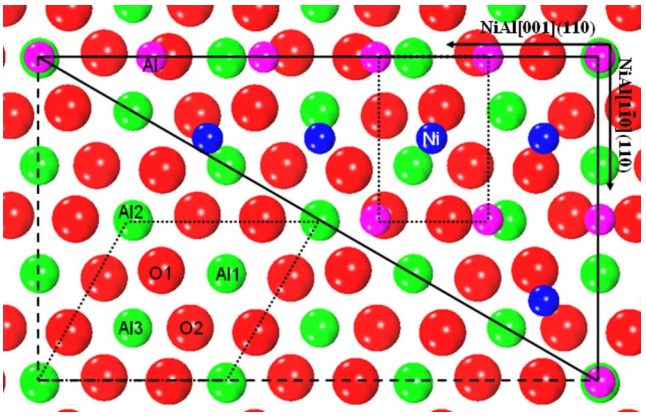

FIG. 1. (Color online) Top view of the model 1 interface supercell. Only half of the Ni-Al overlayer (small balls) is shown. Al1 and Al2 indicate the sites for top Al layer nearest to or next nearest to the oxygen layer and Al3 for the Al layer just beneath the oxygen (O1) layer. The O1 and O2 label the two sequential close-packed oxygen layers following an *A-B-A-B* pattern in Al_2O_3 while Al1, Al2, and Al3 are for the three sequential Al layers following an *A-B-C* pattern. The small rectangle indicates the Ni-Al (110) 1×1 primitive cell and the rhombus the α-Al_2O_3 (0001) 1×1 primitive cell. Al atoms in Al_2O_3 is green, O is red, Al in Ni-Al is pink, and Ni is blue.

a reliable comparison of calculations for different interfaces, all calculations were performed using the same supercell dimensions. Similar to our earlier work,[34] the interfacial energy is defined by subtracting from the total energy of an interface ensemble the contributions of two bulk materials *subject to the same imposed strain*.

B. Models of the β-$Ni_{1-x}Al_x$/ α-Al_2O_3 interface

Our model of the β-$Ni_{1-x}Al_x$/ α-Al_2O_3 interface uses the following supercell geometry. The supercell contains a vacuum area of ~10 Å thickness and a five-layer Ni-Al (110) slab placed on a four O-layer α-Al_2O_3 (0001) slab. Periodicity is invoked parallel to the interface plane, a virtual plane separating the Ni-Al alloy from the oxide. The interface orientation of Ni-Al (110) matching Al_2O_3 (0001) has been investigated quite often in experiments.[35–39] However, within those interfacial mismatches, there are a few potential models of the interface with different planar matching or orientation. Traditionally, the model interface for *ab initio* studies is constructed seeking the configuration with minimum interfacial mismatch,[19,21,32–34,40,41] and usually the material with the smaller modulus is deformed into commensuration with the stiffer material.[19,21,33,40,41] It has been demonstrated that the model interface built in this way reproduces well the chemical-bonding characteristics, stability, and mechanical properties of the experimental interface.[42] This is the approach we followed to build the model 1 interface (see Fig. 1). However, there are a few other models of the interface with different planar mismatches. Among them, models 2 and 3 (see Fig. 2 below) are the most likely candidates considering the fact that configurations similar to models 2 and 3 were adopted in the study of the interfaces between β-NiAl and Al_2O_3 film.

Model 1. The Ni-Al and Al_2O_3 slabs are in commensuration as NiAl$[1\bar{1}0](110)\|\alpha$-Al_2O_3 $[10\bar{1}0]$ (0001) and Ni-Al [001] (110)$\|\alpha$-Al_2O_3 $[\bar{1}2\bar{1}0]$ (0001). This results in an interface unit cell in which Ni-Al (110) (5×2) matches Al_2O_3 (0001) $(3\times\sqrt{3})$ cells, as shown in Fig. 1. Of the three possible models, this interface possesses relatively low interface mismatch and thus low strains for the two bulk slabs. By taking the lattice constant of Ni-Al to be 2.887 Å,[4] and that of α-Al_2O_3 to be 4.7628 Å,[31] the interface could be built by compressing Ni-Al (110) 1.02% in [001] direction and stretching 1.03% in $[1\bar{1}0]$ direction to match Al_2O_3 (0001). Earlier work on metal/Al_2O_3 interfaces by a number of researchers showed that such a low mismatch is helpful in obtaining reliable interface stability trends as well as for analyzing chemical bonds.[19,21,40–42]

Model 2. Considering the so-called Kurdjumov-Sachs (KS) orientation relationship between fcc (111) and bcc (110) meshes,[43–45] model 2 (quasi-KS orientation) is constructed by aligning the close-packed Ni-Al line of the Ni-Al (110) with the closed-packed oxygen line of the α-Al_2O_3 (0001), as shown in Figs. 2(a) and 2(c). There are 11 Ni-Al primitive cells and a $3\times\sqrt{3}Al_2O_3$ cell in the in-plane interface unit cell. The two sides of the Ni-Al rectangle are compressed by 4.75% to match the α-Al_2O_3 (0001) at this configuration. There is an angular deformation of 3.7° as shown in Figs. 2(a) and 2(c).

Model 3. This model is similar to the so-called "row-matching" orientation,[35] with which a model interface could be built through deforming and removing a Ni-Al cell from Ni-Al slab, as shown in Figs. 2(b) and 2(c). Based on that, Kresse *et al.*[16] had built an interface between β-NiAl and *ultrathin* Al_2O_3 through displacing a Ni-Al primitive cell into the fixed substrate mode. For testing purposes in the current work, a quasirow-matching interface is also built through displacing a Ni-Al primitive cell from the Ni-Al slab to match the fixed Al_2O_3. There are 15 Ni-Al primitive cells and an $2\times2\sqrt{3}Al_2O_3$ cell in the in-plane interface unit cell, as shown in Figs. 2(b) and 2(c). The two sides of the Ni-Al rectangle are compressed 10.75% and 0.51%, respectively, together with an angular deformation of 2.7° as shown in Fig. 2.

Generally speaking, the model 2 and model 3 configurations are not expected to exist for the interface between *thick* Al_2O_3 and $Ni_{1-x}Al_x$ alloy due to the relatively high internal strains. This seems to be consistent with the recent experimental observation of the stable existence of the model 1 interface between Ni-Al and thick α-Al_2O_3 by Stierle and co-workers.[46] To further check the relative stability, a typical model interface between a stoichiometric five-layer Ni-Al slab and an Al-terminated Al_2O_3 slab [labeled as $(Al_2O_3)_{Al}$] at each specific orientations (models 1, 2, and 3) is built. The interfacial energies for the three prototype interfaces are calculated and presented in Table I. It is clear that the model 1 interface has the lowest interfacial energy value, which is consistent with the aforementioned principle of minimum mismatch and leads us to conclude that model 1 is the best choice among the three models when considering the effects of both the lattice mismatch and the magnitude of the interface energy. Therefore, the orientation of model 1 is employed for all following calculations.

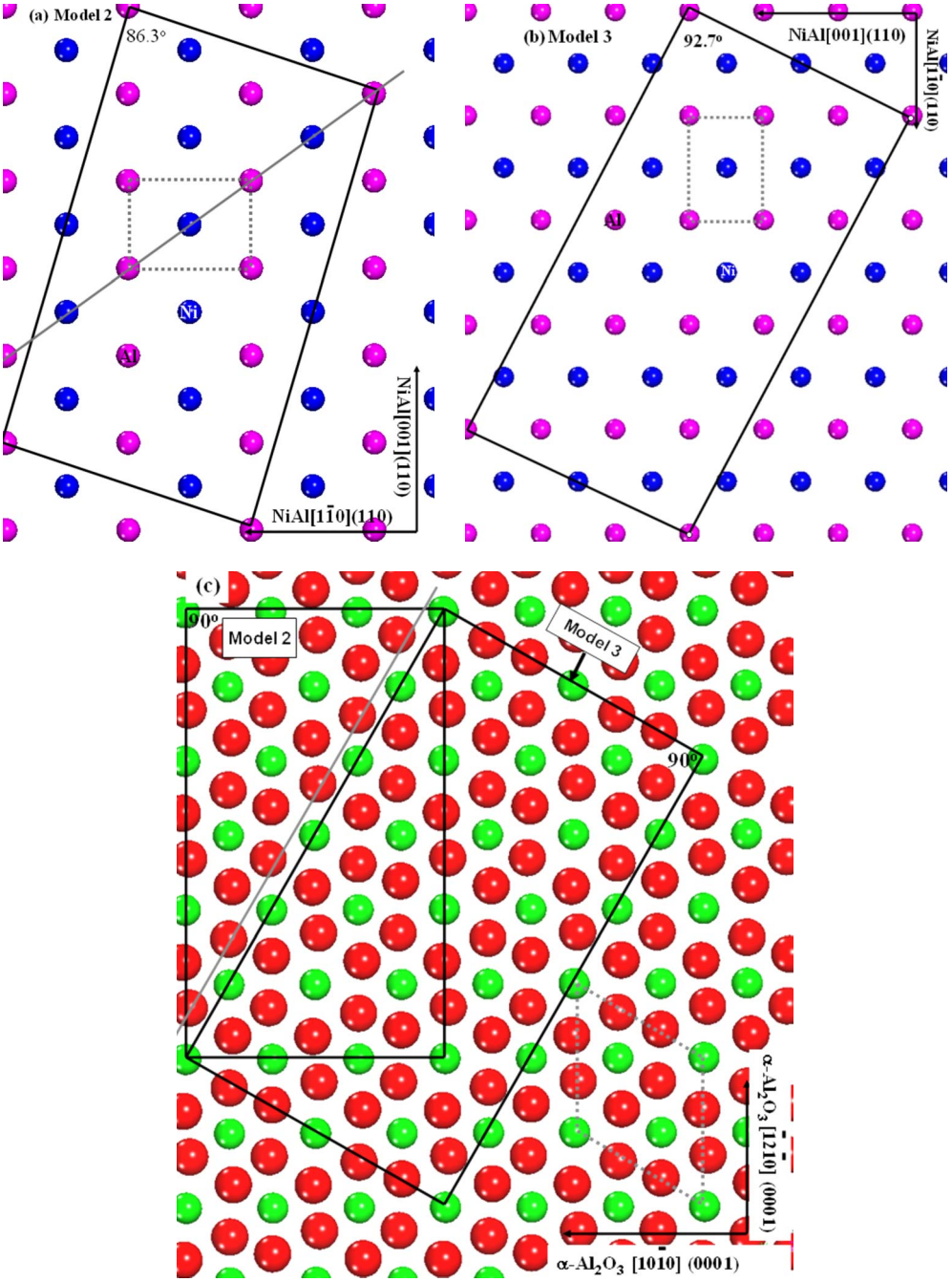

FIG. 2. (Color online) (a) and (b) show the top view of the models 2 and 3 on Ni-Al (110) surface; (c) exhibits models 2 and 3 on α-Al_2O_3 (0001). The small rectangle indicates the Ni-Al(110) 1×1 primitive cell and the rhombus the α-Al_2O_3 (0001) 1×1 primitive cell. The grey line in (a) and that in (c) indicates the close-packed Ni-Al line of Ni-Al (110) and the closed-packed oxygen line of α-Al_2O_3 (0001), respectively. Al atoms in Al_2O_3 is green, O is red, Al in Ni-Al is pink, and Ni is blue.

Starting from the model 1 interface with Ni-Al (110) (5×2) matching α-Al_2O_3 (0001) $(3\times\sqrt{3})$, various interfaces at different chemical compositions are built for detailed investigations. The Al_2O_3 surface can have Al_2, Al, or O termination. While the different surfaces are labeled as $(Al_2O_3)_{Al2}$, $(Al_2O_3)_{Al}$, or $(Al_2O_3)_O$, the corresponding interfaces with the Al_2, Al, or O termination of the Al_2O_3 scale are labeled as Al_2*term*, Al*term*, or O*term*, respectively. The Al_2 termination is characterized by an α-Al_2O_3 (0001) surface terminated by two layers of Al atoms occupying the Al1 and Al2 sites (see Fig. 1). The Al termination and O termination pertain, respectively, to an α-Al_2O_3(0001) terminated by a single layer of Al atoms at Al1 sites, and by a single layer of oxygen atoms. In order to avoid obtaining metastable states of complex interfaces, ten initial configurations are built by sliding the Ni-Al overlayer on the Al_2O_3 surface and matching a specified Ni (or Al) atom to Al1, Al2, Al3, O1, or O2 positions (see Fig. 1), respectively. After full relaxation of the initial configurations, three *as-relaxed* stable interface structures with lowest total energies for the three

TABLE I. Three possible models of the $NiAl/Al_2O_3$ interfaces with different orientations and mismatch are shown. The interfacial energy of an interface between a stoichiometric Ni-Al layer and an Al-terminated $(Al_2O_3)_{Al1}$ slab at each of the three orientations is calculated and listed. The "+" and "−" represent the status of lattice stretching (+) or compressing (−), respectively.

Model	Orientation relationship	Mismatch by Ni-Al (110)	Interfacial energy (J/m^2)
1	$NiAl[1\bar{1}0]\|\|Al_2O_3[10\bar{1}0]$	+1.03% in $[1\bar{1}0]$	
	$NiAl[001]\|\|Al_2O_3[\bar{1}2\bar{1}0]$	−1.02% in [001] degree 0°	2.37
2	Quasi-KS orientation	−4.75% in long side	
		−4.75% in short side degree 3.7°	3.22
3	Quasirow-matching orientation	−10.75% in long side	
		−0.51% in short side degree 2.7°	16.95

terminations are obtained. Based on the three *as-relaxed* configurations, additional operations are also performed to search for other possible stable interfaces. One operation is to remove Al atoms in interface layers one by one to change the interfacial chemical composition; the other is to exchange interfacial Al (Ni) atoms with Ni (Al) atoms in both atomic layers close to interface plane and bulk Ni-Al. Change in the Ni stoichiometry by removing/adding 1–2 Ni atoms from/to each configuration is also considered, although the normal process to grow an Al_2O_3 scale through oxidization of the Ni-Al alloy can be expected not to change the number of Ni atoms. By searching over the terminations and compositions in a systematic way, the aforementioned manipulations could help us to figure out the most important interfacial configurations of various chemical compositions. An example which may help to explain our notation is O*term*-8Al that represents the most stable, optimized O-terminated structure with eight Al atoms removed from the *as-relaxed* initial configuration of O termination. Al_2*term*-1Al indicates a stable configuration from the Al_2-terminated oxide scale with one Al atom removed from the *as-relaxed* structure.

C. Total energy employing interface representative layers

Our intention is to deal with the interface between the β-$Ni_{1-x}Al_x$ alloy and the thick α-Al_2O_3 around $x \sim 0.5$. Unlike, e.g., the Ni/Al_2O_3 interface for which the *ab initio* Gibbs energy of the interface ensemble is well defined from a supercell calculation, the β-$Ni_{1-x}Al_x/\alpha$-Al_2O_3 interface requires an approximation because the total energy G_{total} of the interface, i.e., the first term of the right side of Eq. (3), also depends on the alloy composition x. To deal with the alloy/Al_2O_3 interface, we need to introduce the concept of *interface representative layers* that describe some atomic layers close to the virtual interface plane separating alloy from oxide. The important point is that the *interface representative layers* are considered to be similar and stable at a local equilibrium when x deviates slightly from stoichiometry ($x=0.5$) in the β-$Ni_{1-x}Al_x$. A few points make this approach reasonable. On the one hand, only alloys with compositions close to $x=0.5$ are considered in this work. Chemical bonding in the stable $Ni_{1-x}Al_x$ alloy with a limited composition deviation changes slightly in comparison with that in the strictly stoichiometric β-NiAl. On the other hand, the local structure of an interface is mostly determined by the local bonding in the *interface representative layers* which retain the most important information of chemical bonding of the interface. This is especially true when the interfacial energy is estimated by subtracting the contributions of the strained bulks from the energy of interface ensemble in our calculations.

Based on the approximation of the *interface representative layers* for alloy/Al_2O_3 interface, a supercell (see Fig. 3) is built for *ab initio* calculations. The supercell contains four regions. Region 1 is $> \sim 10$ Å vacuum layer. Regions 2 and 4 are the bulk β-$Ni_{1-x}Al_x$ alloy and the bulk Al_2O_3, respectively. Region 3 indicates the *interface representative layers* designed to simulate various interfacial compositions obtained through operations as discussed in above Sec. III B. Usually, the *interface representative layers* are composed of 3–4 Ni-Al layers and 2-oxygen-layer Al_2O_3 slab. Region 2 is used to represent the bulk Ni-Al alloy with a fixed composition and its contribution will be subtracted from the self-consistent total energy of the supercell for interfacial stability analysis. With this, the G_{total} for Eq. (3) can be obtained by

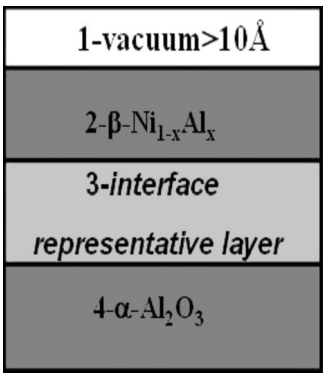

FIG. 3. Schematic supercell of a model interface for *ab initio* calculations. Regions 1, 2, 3, and 4 represent vacuum, β-$Ni_{1-x}Al_x$, *interface representative layer*s, and bulk α-Al_2O_3, respectively. By introducing the *interface representative layer*s for simulating alloy-oxide interface, region 2 could be replaced by a stoichiometric β-NiAl layer as a reference substrate in practical calculations.

$$G_{total} = E_{total} - E_1 - E_2(x=0.5) - E_4. \quad (4)$$

Here E_{total} is the total energy of the supercell. E_1, E_2, and E_4 refer to the total energies of regions 1, 2, and 4, respectively. Because we focus on those interfaces between α-Al_2O_3 and a stable β-$Ni_{1-x}Al_x$ phase with a limited composition deviation from the strictly stoichiometric case, region 2 for all interface configurations is represented by a slab of stoichiometric β-NiAl (x=0.5) subject to the same imposed strain as the interface. This slab is defined as the *reference substrate*. The other *reference substrate* is the bulk Al_2O_3 (region 4). Therefore, E_1, E_2, and E_4 in Eq. (4) are just the sum of two surface energies, total energy of the strained bulk β-NiAl (x=0.5), and that of the bulk α-Al_2O_3. A few test calculations show that replacing the stoichiometric *reference substrate* in region 2 by alloys with slight deviations of x from 0.5 shows no effects on the final interfacial relaxation in the fully relaxed supercell. After subtracting the contributions of the regions 1, 2, and 4 (E_1, E_2, and E_4) from the total energy of the supercell, the remainder is the energy of the central layers, i.e., the *interface representative layers*, retaining the most important information of chemical bonding of the interface. This energy term is retained in the G_{total}, which is used for composition-dependent stability analysis.

D. Chemical potential $\mu_{Ni_{1-x}Al_x}$

In our approach, the chemical potential $\mu_{Ni_{1-x}Al_x}$ in Eq. (3) is given by

$$\mu_{Ni_{1-x}Al_x} = (1-x)\mu^0_{Ni} + x\mu^0_{Al} + \Delta H_{Ni_{1-x}Al_x}(0\ \mathrm{K}), \quad (5)$$

where μ^0_{Ni} and μ^0_{Al} are the chemical potentials of bulk Ni and Al at 0 K. $\Delta H_{Ni_{1-x}Al_x}$ is the formation enthalpy of β-$Ni_{1-x}Al_x$ at 0 K. Because there exists a linear relationship between $\Delta H_{Ni_{1-x}Al_x}$ and the bulk composition x,[47] the $\Delta H_{Ni_{1-x}Al_x}$ is interrelated by

$$\Delta H_{Ni_{1-x}Al_x} = \Delta H_{Ni_{1-x}Al_x}(x=0.5) + c_1(x-0.5) \quad (x<0.5),$$

$$\Delta H_{Ni_{1-x}Al_x} = \Delta H_{Ni_{1-x}Al_x}(x=0.5) + c_2(x-0.5) \quad (x>0.5). \quad (6)$$

The measured formation enthalpy of β-$Ni_{1-x}Al_x$ alloy at different temperatures showed that temperature has a minor effect on the functional relationship, and the coefficients c_1 and c_2 are estimated to be −1.13 and 0.72 eV by fitting to the experimental data (see Fig. 1 of Ref. 47). The formation enthalpy $\Delta H_{Ni_{1-x}Al_x}$ (x=0.5) is calculated to be −0.64 eV/atom (−61.72 kJ/mol), in good agreement with experimental data of -62 ± 2 kJ/mol.[47] Figure 4 shows the relationship between the estimated $\mu_{Ni_{1-x}Al_x}$ and the alloy composition x based on Eqs. (5) and (6). *Ab initio* calculations of the formation enthalpies are also carried out for $Ni_{1-x}Al_x$ alloys at the two compositions of x=0.468 and 0.517, and the results are also labeled in Fig. 4. For that, a $5\times5\times5$ supercell approach to Ni-Al is used. The composition deviation from 0.5 is realized by introducing Ni vacancies for the Al-rich and Ni antisite atoms for the Ni-rich Ni-Al alloys.[48] These calculated formation enthalpies agree well with available experimental data.[47]

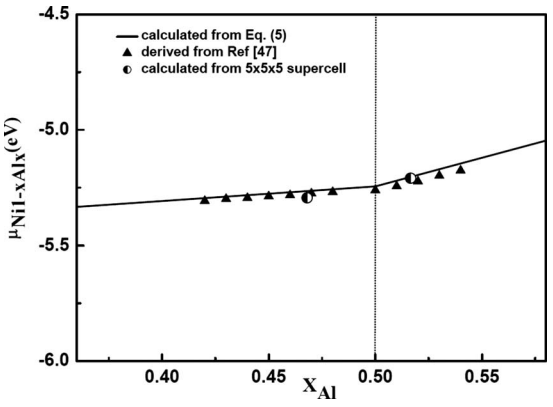

FIG. 4. Relationship between $\mu_{Ni_{1-x}Al_x}$ and x. The solid line is from Eqs. (5) and (6). The coefficients in Eq. (6) are obtained by fitting to the available experimental data (filled triangles) from Ref. 47. The half-filled circles label the calculated values by a $5\times5\times5$ supercell approach to β-$Ni_{1-x}Al_x$ alloy at x=0.468 and 0.517, and details are described in the text.

E. *Ab initio* effective chemical-potential difference $\Delta\mu_{Al}$

In *ab initio* computations combining thermodynamics,[18] the effective chemical-potential difference $\Delta\mu_{Al}$ of Al in Eq. (3) is related to the Al activity a_{Al} by

$$\Delta\mu_{Al} = k_B T \ln a_{Al} + \Delta^0_{Al}(T), \quad (7)$$

$$\Delta^0_{Al}(T) = \mu^0_{Al}(T) - \mu^0_{Al}(0\ \mathrm{K}), \quad (8)$$

where k_B is the Boltzmann's constant. $\mu^0_{Al}(T)$ corresponds to the chemical potential of a thermodynamic standard state of solid Al at temperature T. $\mu^0_{Al}(0\ \mathrm{K})$ is the total energy of per Al atom of solid Al at 0 K. Here, the connection energy $\Delta^0_{Al}(T)$ can be calculated by the approach as suggested in Ref. 18 or by using the data from the JANAF Thermochemical Tables.[49] Linking a_{Al} and x, Meyer *et al.*[17] have put forward a relationship between them as

$$\ln\frac{a_{Al}(x_{Al})}{a_{Al}(x_{Al}=0.5)} = \begin{cases} -\frac{1}{6}G_0/k_BT - \frac{1}{3}\ln 2 + \frac{1}{2}\ln\frac{4x^2_{Al}}{1-2x_{Al}} & (x_{Al}<0.5) \\ \frac{1}{3}G_0/k_BT - \frac{1}{3}\ln 2 + \ln\frac{2x_{Al}-1}{x_{Al}} & (x_{Al}>0.5) \end{cases} \quad (9)$$

in which G_0 is a constant. $\ln a_{Al}(x_{Al}=0.5)$ can be taken to be −6.88 from Ref. 50. By substituting Eqs. (8) and (9) into Eq. (7), the relationship between $\Delta\mu_{Al}$ and x can be established. Finnis *et al.*[51] also derived a similar function linking $\Delta\mu_{Al}$ with the alloy composition x. Although a complex triple defect system or defect clustering effect is considered in Meyer's approach but not in Finnis's model, both approaches agree with each other well for the estimated trend of $\Delta\mu_{Al}$ vs x and only manifest slight differences, as plotted in Fig. 5. Considering the fact that Meyer's model reproduces well the experimentally measured x dependence of the Al activity in

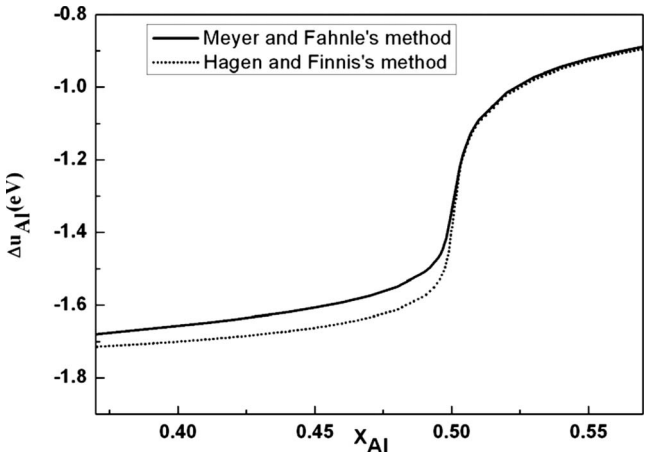

FIG. 5. The effective chemical-potential difference $\Delta\mu_{Al}$ versus bulk alloy composition x.

Ni-Al alloy, the approach is chosen for our simulations. Because the experimental data measured at 1273 K were used to validate the relationship between the Al activity and alloy composition x,[17] we chose the same temperature for our discussions (see Fig. 5).

IV. RESULTS AND DISCUSSIONS

A. Interface stability

Interfacial energies γ_I of several typical configurations are calculated for different terminations of the α-Al_2O_3/β-$Ni_{1-x}Al_x$-alloy interfaces. In a practical environment, equilibrium between an ambient gas species and solid interface implies that the chemical potentials of species in the gas and the corresponding species at the interface are the same. So the ambient gas O_2 partial pressure p_{O_2} can be given by

$$\ln p_{O_2} = \frac{2}{3}\left[\frac{1}{k_B T}\Delta G_{Al_2O_3}(T) - 2\ln a_{Al}\right]. \quad (10)$$

Here, $\Delta G_{Al_2O_3}(T)$ is the Gibbs formation energy of α-Al_2O_3 at given temperature, which can be estimated from JANAF tables[49] or other handbooks. By combining Eqs. (9) and (10), the oxygen partial pressure p_{O_2} can be linked to alloy composition x. The $Ni_{1-x}Al_x$ alloy exists as a well-ordered β phase in the range of x from 0.369 to 0.571 at 1273 K according to phase diagram analysis.[52] The interfacial energies γ_I of different configurations as a function of x or p_{O_2} are presented in Fig. 6. This plot clearly demonstrates that the interface energies γ_I may change drastically around the composition x=0.5. From Fig. 6, it can be concluded that there may exist two types of stable configurations for the β-$Ni_{1-x}Al_x$/α-Al_2O_3 interfaces. One type is obtained by joining the Al-rich Ni-Al alloy with the Al_2-terminated Al_2O_3 surface, possibly with some interfacial Al atoms removed. Among all possible configurations investigated, the Al_2*term*-1Al shows the lowest interface energy (type I). The other type of the interface could be speculated to be obtained through the combination of a Ni-rich Ni-Al alloy with the

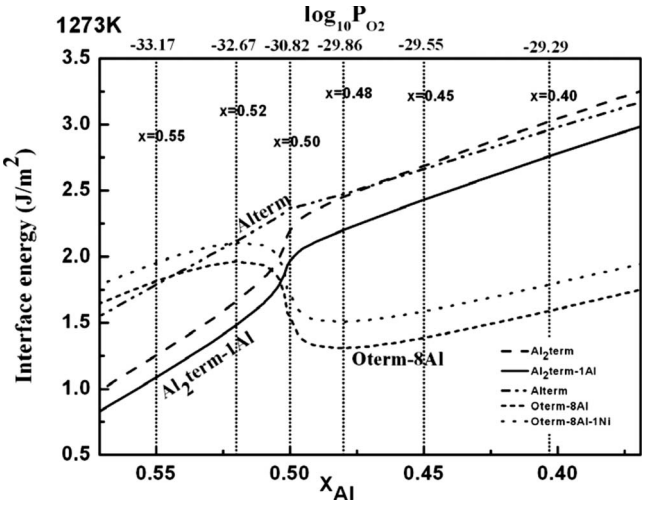

FIG. 6. Interfacial energies γ_I of several typical configurations of the β-$Ni_{1-x}Al_x$/α-Al_2O_3 interface as a function of bulk composition x and oxygen partial pressure P_{O_2} at 1273 K.

O-terminated Al_2O_3 surface. In the process of forming a stable interface, our simulations show that Al atoms located in the Ni-Al bulk region have a strong tendency to migrate to get into contact with oxygen atoms at the interface, which leads to the formation of a Ni-rich layer at the interface. Meanwhile, our calculations also show that removing a few Al atoms from the Ni-rich layer could release the strain within it and help to stabilize the layer. Among many configurations calculated, the O*term*-8Al interface, with eight Al atoms removed, shows the lowest interfacial energy (type II). There is no guarantee that all possible interfacial configurations have been considered, due to the complexity of such an alloy/oxide interface. The general tendency of the interfacial stability is believed to be correctly revealed because so many configurations of different chemical compositions have been tested in a systematic way, however. For $x>0.503$, the Al_2*term*-1Al is the most stable interface, and the O*term*-8Al is the most stable configuration when $x<0.503$. Compared with the Al_2*term*-1Al and O*term*-8Al interfaces, the interfaces with initially a single Al-layer termination of the Al_2O_3 scale are unstable in terms of the calculated interfacial energies (see Fig. 6).

Figure 6 also shows the relationship between the calculated interfacial energy and the oxygen partial pressure. In principle, this implies that a global thermodynamic equilibrium has been reached and that the thermodynamic state variables are time independent and that the chemical potential μ_i of each species is position independent. This may not be true for an entire system in practice but nevertheless a local equilibrium may be assumed in some cases. For example, for an interface it is reasonable to assume that there is a local thermodynamic equilibrium on the atomic scale between the interface region and a region of the bulk materials in the vicinity of the interface.[53] This assumed equilibrium region might be broadened to include the ambient gas so that the ambient gas partial pressures as well as the activities of material components could be included as useful thermodynamic variables. In some cases, the measured chemical-

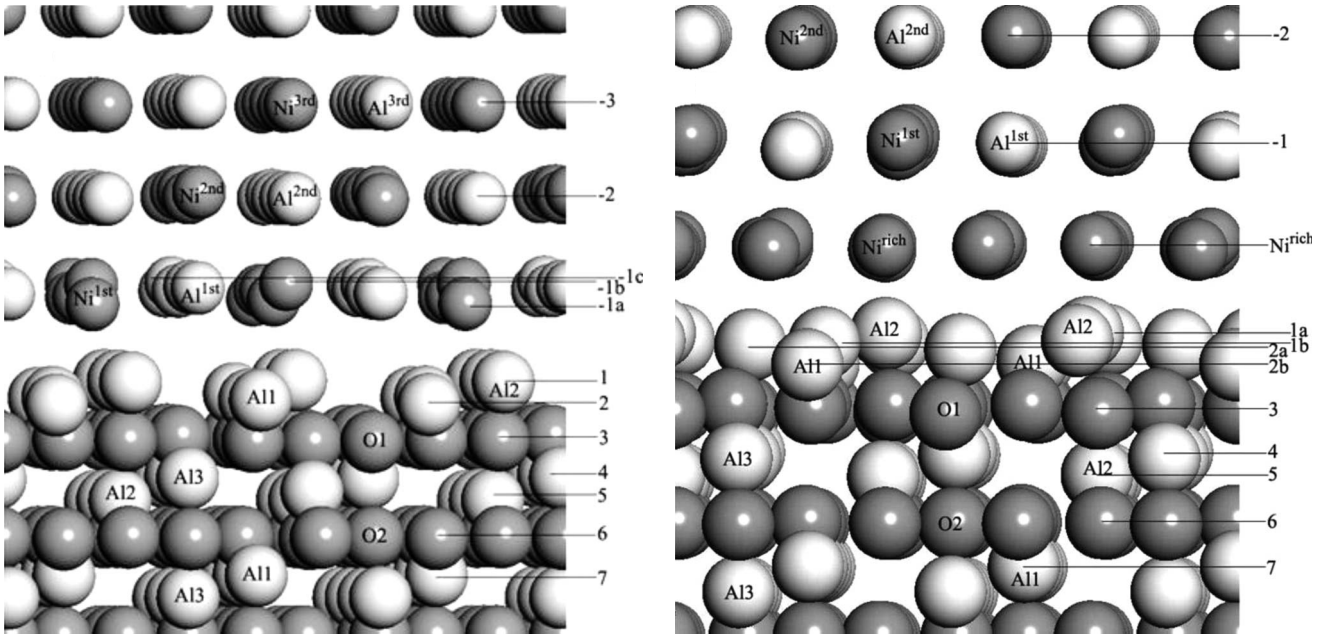

FIG. 7. The optimized structure of the two stable interfaces. (a) Type-I Al_2*term*-1Al interface. The −1a and −1b denote the lowest and highest Ni atoms in the first Ni-Al layer, respectively, and the −1c indicates the highest Al atom in the first Ni-Al layer; (b) Type-II O*term*-8Al interface. The 1a and 1b denote the highest and lowest Al2 sites, respectively, and the 2a and 2b are used to label Al1 sites similarly. Other types of atoms are indicated in the figures.

potential gradient may even be applied to determine the local partial pressure of material components. From this point of view, those results (Fig. 6) are also helpful for understanding the structural stability of an interface in local equilibrium with the bulk regions on either side of the interface.

B. Interfacial structure and chemical bonding

1. Al_2term-1Al interface

The fully relaxed atomic structure of the type-I Al_2*term*-1Al interface is shown in Fig. 7(a). Because of the rumpling of the first Ni-Al layer (−1 layer) in the Ni-Al slab, three typical sublayers in the layer are labeled as −1a, −1b, and −1c, respectively. The spacing between the highest and lowest Ni atoms (degree of rumpling) is 0.44 Å (see Table II). Notice that the interplanar distance between the −1c and −1a sites is only ~0.46 Å, implying that the roughness of the first Ni-Al layer is relatively small. Although the first Ni-Al layer buckles, as a whole, the other layers in the Ni-Al slab, even in the vicinity of interface plane, are weakly influenced by the formation of an interface with the oxide scale. This is a feature of the type-I interface, most likely due to the fact that the Al_2O_3 surface is covered well by Al atoms in order to saturate the oxygen dangling bonds on the surface. Similar to the Al-rich cases in $(Ni,Cu)/Al_2O_3$ interfaces as we studied before,[34] Al atoms continue epitaxially occupying the Al1 and Al2 sites of the Al_2O_3 surface at the type-I interface but with changed interlayer spacings (see Table II). The second (−2) and third (−3) Ni-Al layers in the Ni-Al slab exhibit a displacement of ~0.20 Å along the Ni-Al $[1\bar{1}0]$ direction with no obvious change in the intra-planar and interplanar atomic positions after relaxation, assuming that the bulk spacing from the strained Ni-Al is used in the initial configuration. This rapid decay of relaxation with distance from the interface demonstrates the validity of taking only a few Ni-Al (110) and Al_2O_3(0001) layers as the *interface representative layers* for our calculations. Table II displays the spacing between the atomic planes as indicated in Fig. 7(a). The spacing between layer 1 and layer 2 (in Al_2O_3) is compressed 18.37% in comparison with the bulk value in Al_2O_3 while the distances between other planes

TABLE II. Interfacial spacings (in Å) for a type-I Al_2*term*-1Al interface and a comparison with bulk values. The interfacial layers are labeled as shown in Fig. 7(a).

Al_2*term*-1Al interface			
Atomic layer	Interface spacing	Bulk spacing	Bulk differential (%)
(−3,−2)	2.05	2.05	+0.00
(−2,−1c)	1.92	2.05	−6.34
(−1c,−1b)	0.02	0.00	
(−1b,−1a)	0.44	0.00	
(−1a,1)	1.69		
(1,2)	0.40	0.49	−18.37
(2,3)	0.87	0.84	+3.57
(3,4)	0.87	0.84	+3.57
(4,5)	0.48	0.49	−2.04
(5,6)	0.85	0.84	+1.19
(6,7)	0.85	0.84	+1.19

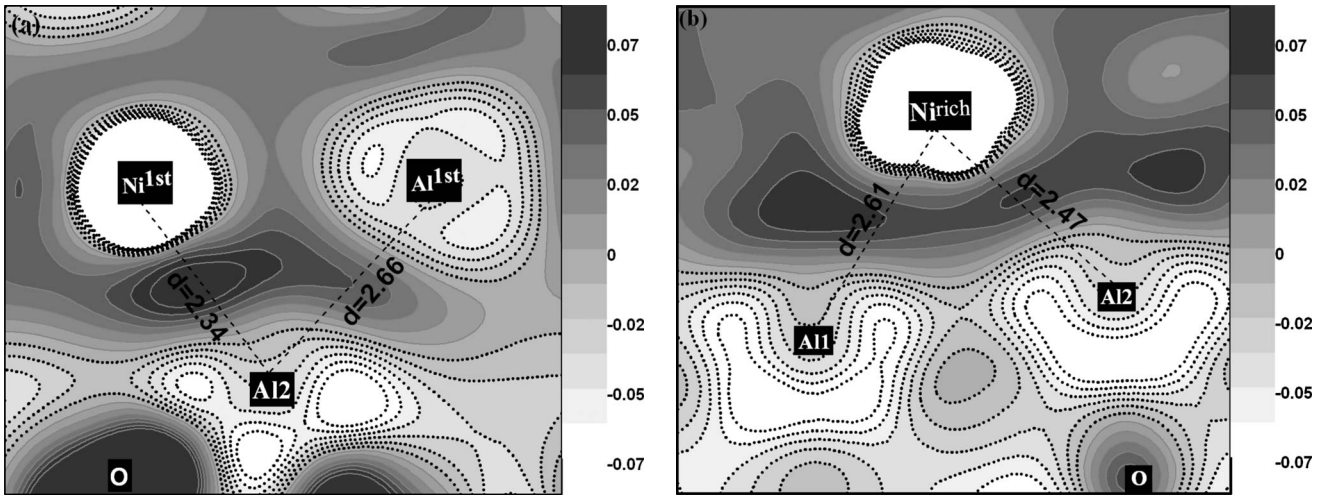

FIG. 8. Contour plots of valence electron-density difference for the type-I and type-II interfaces. (a) Type-I Al_2*term*-1Al interface: the plane across Ni^{1st}, Al^{1st}, Al2, and O atoms as labeled in Fig. 7(a); (b) type-II O*term*-8Al interface: the plane across Ni^{rich}, Al1, Al2, and O atoms as indicated in Fig. 7(b). The dark gray areas with solid lines indicate electron accumulation and the light gray areas with short dot lines indicate electron depletion. The distances *d* (short-dashed lines) denote the distance (in Angstroms) between the atoms linked. The unit of charge density is $e/Å^3$.

change little. As for the positions of atoms in the Ni-Al slab relative to the oxide, it seems that Ni atoms prefer to locate on top of Al atoms (Al1 and Al2) of the oxide layer for all configurations studied, which indicates that Ni atoms at the interface tend to form chemical bonds with Al atoms from the Al_2O_3 layer. A similar conclusion was also obtained by others through combining scanning tunneling microscopy observations with *ab initio* calculations.[16] Our results prove that the Ni-Al alloy may form a sharp interface with α-Al_2O_3 at an appropriate condition. Indeed, the ultimate stable and thick α-Al_2O_3 phase was detected in a recent experiment during the oxidation of Ni-Al (110) with well-defined interface matching.[46] This is consistent with our theoretical prediction. Finally, it is noted that there is no requirement for antisite atoms to exist at the Al_2*term*-1Al interface, consistent with the earlier investigation of Kresse *et al.* for a similar interface.[16]

Insight into the chemical bonding nature at an interface can be obtained by examining the valence electron-density difference (VEDD), and the result for the Al_2*term*-1Al interface is shown in Fig. 8(a). The valence electron-density difference is calculated by subtracting the superposition of valence electron densities of neutral atoms from the self-consistent charge-density distribution of the fully relaxed interface. Figure 8(a) shows a result for a plane across the Ni^{1st}, Al^{1st}, Al2, and O atoms [see Fig. 7(a)]. The Ni^{1st} and Al^{1st} atoms are from the first Ni-Al layer, and the Al2 atom (at the highest Al2 site) and the O atom from the Al_2O_3 surface. This is a typical configuration for the Al_2*term*-1Al interface. Here, the Ni^{1st}-Al2 distance is 2.34 Å and that for Al^{1st}-Al2 is 2.66 Å, a little shorter than the nearest Ni-Al (2.50 Å) and Al-Al (2.89 Å) distances in bulk Ni-Al. In addition, there is obvious charge transfer from the Al atoms at interface to oxygen atoms in Al_2O_3, indicating the strong ionic characteristic of chemical bonding in the type-I interface. However, the slightly changed Al1-O distances in Al_2O_3 (see Table II), in comparing with those interlayer spacings in bulk Al_2O_3,[34] indicate that the adhered Ni-Al slab does affect the bonding in the Al_2O_3 slab to some extent, mainly in the area close to the interface. It can also be observed that there is charge accumulation between Ni^{1st} (Al^{1st}) in Ni-Al and Al2 in Al_2O_3, relatively close to Ni atoms, indicating the existence of direct chemical interaction between the Ni^{1st} (Al^{1st}) from the Ni-Al slab and the Al2 from Al_2O_3. The charge redistribution between Ni^{1st} (Al^{1st}) and Al2 atoms shows a quite extended spatial distribution, implying the characteristic of metallic bonding at the interface. The interaction between Ni^{1st} and Al2 probably also includes a small amount of covalent bonding, as indicated by the charge-density redistribution pattern. Overall, the metallic interaction is still dominant. VEDD for other pairs of atoms at the interface, such as Ni^{1st}-$Al1_{(Al2O3)}$ and Al^{1st}-$Al1_{(Al2O3)}$, also exhibits a pattern similar to the above-discussed picture about the typical Ni^{1st} (Al^{1st})-$Al2_{(Al2O3)}$ interaction. Generally speaking, the chemical bonding at the type-I Al_2*term*-1Al interface is clearly ionic close to the Al_2O_3 and then metallic between the Ni-Al slab and the Al-covered Al_2O_3 surface.

2. Oterm-8Al interface

The most striking characteristics of the stable type-II O*term*-8Al interface have two aspects, as shown by the ball model of the fully optimized atomic structure of the interface [see Fig. 7(b)]. First there are plenty of Al atoms on top of the originally O-terminated Al_2O_3 surface, which makes the interface also Al rich. Secondly, there exists a Ni-rich layer close to the interface. Those interfacial Al atoms, as labeled also by Al1 and Al2 in Fig. 7(b), are initially located inside the Ni-Al slab, and some of them are actually not even in close contact with Al_2O_3 surface. During the interface structure optimization, those Al atoms show a strong tendency to exchange their positions with Ni atoms that are in close contact with Al_2O_3, tending to occupy the specific epitaxial Al1,

Al2 or nearby sites on the Al_2O_3 surface, and saturating the dangling oxygen bonds of the O-terminated Al_2O_3 surface. Most of the site exchange of atoms is realized through the use of different initial interfacial configurations, which makes the search for stable type-II interface tedious. However, after the Al atoms from the first Ni-Al layer closely interacting with Al_2O_3 in the initial configuration are used up, the tendency of the Al atoms to migrate from a deep Ni-Al layer to the O-terminated Al_2O_3 surface is also very strong, until all the dangling oxygen bonds are saturated in order to lower the interfacial energy. The atomic relaxation leads to a spontaneous formation of the Ni-rich layer through exchanging of atoms and merging of atomic layers in the initially O-terminated Al_2O_3/NiAl-alloy interface. Two points need clarification. First, those Al atoms at the type-II O*term*-8Al interface do not perfectly occupy the regular Al1 and Al2 sites (epitaxial sites) of the Al_2O_3 surface, as long as the Al-rich layer could form a stable configuration to become compatible with the nearby Ni-rich layer. By counting the site occupancy of the Al atoms in the type-II interfacial layer in a statistical way, nearly two third of the Al atoms occupy the epitaxial Al1 and Al2 sites of the α-Al_2O_3 surface while the remaining one third of them locate atop sublayer O2 atoms. Secondly, the Ni-rich layer comes from the merging of two adjacent layers in the initial Ni-Al slab with some Al atoms migrating away to release interfacial strain. As a matter of fact, those interface configurations with chemical compositions close to the O*term*-8Al, such as the O*term*-8Al-1Ni and O*term*-7Al configurations, all have interfacial energies close to each other based on our calculations. For the stable type-II interface, which we know is an Al-rich layer covering the O-terminated Al_2O_3 surface followed by a Ni-rich layer. Our calculations show the O*term*-8Al interface with an ideally clean Ni-rich layer as a typical example. In reality, the Ni-rich transition region may contain more than one atomic layer and may also contain some Al atoms. Indeed, weak double diffraction spots were observed by Libuda *et al.*[54] and were said to support the existence of an additional metallic interlayer between Ni-Al (110) and the oxide film. Furthermore, the appearance of the Ni-rich layers makes it natural for the presence of Ni antisite atoms at the interface, which seems to be consistent with the selective Al oxidation experiments of Ni-Al, in which the α-Al_2O_3 grows predominantly by oxygen inward transport together with Al outward diffusion.[55] The existence of antisite atoms at the Al_2O_3/NiAl interface was also inferred by Stierle *et al.*[14,15] in their early experimental observations.

Considering the obvious rumpling of the Al-rich layers, the sublayers are labeled as 1a, 1b, 2a, and 2b [see Fig. 7(b)], respectively. Compared with the Al_2*term*-1Al interface, the spacings between atomic planes in Al_2O_3 show a substantial change, as exhibited in Table III. The spacing between layers 3 and 4 is expanded by 7.14% in comparison with the corresponding bulk value. The spacing between layers 4 and 5 is compressed by 12.24%.

The nature of chemical bonding at the O*term*-8Al interface can also be extracted from the analysis of the VEDD as plotted in Fig. 8(b). There the VEDD is plotted on a plane through the Ni^{rich}, Al1, Al2, and O atoms. The Ni^{rich} atom is from the Ni-rich layer, and the Al1 and Al2 atoms are from the interfacial Al-rich layer, roughly occupying the specific Al1 and Al2 sites of the oxide surface. Generally speaking, the bonding characteristics in the Al_2*term*-1Al and O*term*-8Al interfaces are quite similar to each other. The Ni^{rich}-$Al1_{(Al2O3)}$ or Ni^{rich}-$Al2_{(Al2O3)}$ interaction is similar to that of the Ni^{1st}-$Al2_{(Al2O3)}$ in type-I Al_2*term*-1Al interface, and could also be regarded as partially covalent and partially metallic, with the metallic component dominant. The dominant metallic characteristics can be observed from the wide spatial distribution of charge-density difference that is located in the area between the Ni-rich and Al-rich layers [see Fig. 8(b)].

TABLE III. Interfacial spacings (in Å) for type-II O*term*-8Al interface and a comparison with bulk values. The interfacial layers are labeled as shown in Fig. 7(b).

O*term*-8Al interface			
Atomic layer	Interface spacing	Bulk spacing	Bulk differential (%)
(−2,−1)	2.03	2.05	−0.98
(−1a,Ni^{rich})	1.99	2.05	−2.93
(Ni^{rich}, 1a)	1.66		
(1a, 1b)	0.20	0.00	
(1b,2a)	0.04	0.49	
(2a,2b)	0.38	0.00	
(2b,3)	0.82	0.84	−2.38
(3,4)	0.90	0.84	+7.14
(4,5)	0.43	0.49	−12.24
(5,6)	0.86	0.84	+2.38
(6,7)	0.85	0.84	+1.19

C. Work of separation W_{sep}

The ideal work of separation W_{sep} is an important fundamental quantity to characterize the mechanical properties of an interface. In principle, it indicates the work to break an interface at a sufficiently high bond-separation rate so that the two resultant surfaces cannot relax to their ground states prior to interfacial bond breaking. The W_{sep} can be given by the difference in total energies between the interface and its separated surfaces as

$$W_{sep} = (E_C + E_D - E_{C/D})/S, \tag{11}$$

where $E_{C/D}$ is the total energy of the interface. E_C and E_D are the total energies of the isolated C or D surfaces after separation, and S is the cross-sectional interfacial area. Table IV lists the typical cleavage modes and the corresponding values of the calculated W_{sep}. $(Al_2O_3)_{Al1}$/Al2-NiAl means that the type-I interface is broken between the Al-terminated surface $(Al_2O_3)_{Al1}$, i.e., Al_2O_3 surface with Al atoms sticking to Al1 sites, and Ni-Al slab with some Al atoms at Al2 sites sticking to it (labeled as Al2-Ni-Al). $(Al_2O_3)_{Al1}$/Al2-Ni^{rich}-NiAl means that the type-II interface is broken between $(Al_2O_3)_{Al1}$ surface and the other part that includes the Ni-rich layer as well as part of the central Al-

TABLE IV. Works of separation W_{sep} (J/m^2) for type-I and type-II $Ni_{1-x}Al_x/\alpha$-Al_2O_3 interfaces are shown. The results for a Ni-Al alloy and Al_2O_3 are calculated for the two bulk regions strained identically as the interface. The work of separation (3.78 J/m^2) for the pure $Ni/(Al_2O_3)_{Al2}$ interface (Ref. 34) is given to compare with that for the interface $(Al_2O_3)_{Al2}/Ni^{rich}$-Ni-Al. Different symbols indicating cleavage planes correspond to the atoms as labeled in Fig. 7.

Interface type	Cleavage plane	W_{sep} (J/m^2)
Al_2*term*-1Al	$(Al_2O_3)_{Al2}/NiAl$	2.85
	$(Al_2O_3)_{Al1}/Al2$-NiAl	2.23 (1.70[a])
O*term*-8Al	$(Al_2O_3)_{Al2}$-$Ni^{rich}/NiAl$	3.26
	$(Al_2O_3)_{Al2}/Ni^{rich}$-NiAl	3.43 (3.78[b])
	$(Al_2O_3)_{Al1}/Al2$-Ni^{rich}-NiAl	2.20 (1.70[a])
Bulk	$(Al_2O_3)_{Al1}/(Al_2O_3)_{Al1}$	3.34 (3.60[b], 3.78[b],3.90[b])
	Ni-Al/Ni-Al	3.38

[a]Reference 56.
[b]Reference 34.

rich layer. $(Al_2O_3)_{Al2}$-$Ni^{rich}/NiAl$ indicates a rupture mode such that the Ni-rich layer remains with the oxide. The other labels in the table are also quite clear and self-explanatory. Among all the cleavage modes, it is always the mode with the $(Al_2O_3)_{Al1}$ surface, the most stable Al-terminated Al_2O_3 surface, that shows the lowest W_{sep} for both type-I [2.23 J/m^2 for $(Al_2O_3)_{Al1}/Al2$-NiAl] and type-II interfaces [2.20 J/m^2 for $(Al_2O_3)_{Al1}/Al2$-Ni^{rich}-NiAl]. It implies that the stability of the β-$Ni_{1-x}Al_x/\alpha$-Al_2O_3 interface is mainly correlated with the mechanical strength of $(Al_2O_3)_{Al1}/X$ adhesion in practice, in which X contains mainly Ni and Al atoms for both the type-I and type-II interfaces. After fully relaxation, the X parts for the two types of interfaces become similar to each other, and therefore the two interfaces show nearly equal values of W_{sep}. This picture is also consistent with the interface chemical-bonding analysis in Sec. IV B, which say that both the type-I and type-II interfaces show dominant metallic-bonding features. This is quite different from the interfaces between Al_2O_3 and single element metals, such as Ni or Cu. In that case, the interfaces of Al and Al_2 termination, i.e. $Ni/(Al_2O_3)_{Al1}$ and $Ni/(Al_2O_3)_{Al2}$ interfaces, manifest metallic bonding while the O-terminated configuration, i.e. the $Ni/(Al_2O_3)_O$ interface, shows relatively strong ionic-covalent bonding.[34] Experimentally, it would be very hard to get reliable W_{sep} data because the exact interface chemical composition is difficult to be characterized. In Table IV, an experimental W_{sep} result (1.70 J/m^2) (Ref. 56) for the $Al_2O_3/NiAl$-alloy interface is listed to compare with the calculated results for both the type-I and type-II interfaces. Considering the uncertainty in both measurements and calculations, the consistency could be considered to be satisfactory. From the calculated W_{sep} data, it is speculated that the interfacial adhesion is relatively weaker than but still comparable to the strength of the Ni-Al alloy and the Al_2O_3 bulk. Therefore, it is possible to break the β-$Ni_{1-x}Al_x/\alpha$-Al_2O_3 adhesion at the interface. When an interface fracture occurs, one part of the resultant surface is the Al_2O_3 surface with Al termination, and the other part should also be partially covered by Al atoms. In addition, the Ni-rich or Al-rich stoichiometries in the Ni-Al alloy should not affect the adhesion of the interface significantly according to our computations while such stoichiometries might affect impurity segregation behavior. Such impurity effects warrant further investigation.

V. SUMMARY

We have carried out an *ab initio* thermodynamics study of the β-$Ni_{1-x}Al_x/\alpha$-Al_2O_3 interfaces with various terminations and chemical compositions. The interfacial energies as well as their dependence on alloy composition, or oxygen partial pressure, reveal that there exist two types of stable interfacial structures. Based on our calculations, they are type-I Al_2*term*-1Al and type-II O*term*-8Al interfaces, although stable configurations may deviate slightly from the theoretically predicted compositions. Both types of interfaces exhibit a common feature of an Al-rich layer on top of the oxide scale while a Ni-rich layer adjacent to the Al-rich layer may be found at the O*term*-8Al interface. The nature of chemical bonding for the two interfaces is thoroughly analyzed via the atomic geometry and electronic structure. It is concluded that the interactions between Ni (and Al) atoms from the Ni-Al slab and Al atoms from oxide, specifically the $Ni\text{-}Al_{(Al2O3)}$ and $Al\text{-}Al_{(Al2O3)}$ interactions at the interfaces, are dominantly metallic with slight covalent characteristics. Our theoretical results for works of separation W_{sep} are reasonable in comparison with available measured and calculated results. A comparison among all possible cleavage modes of the interface suggests that the most likely spallation occurs between an oxide with Al termination and a Ni-Al slab with some extra Al atoms sticking to its surface. Works of separation for possible fractured interfaces are relatively close to each other. Our results could provide a reasonable framework for understanding the interfacial structures and adhesion of the β-$Ni_{1-x}Al_x/\alpha$-Al_2O_3 interface as well as for providing some qualitative guidance for the design of effective Ni-Al-based oxygen diffusion barrier and thermal barrier coatings. One of the interesting results is that the works of separation for the potentially stable interfaces are quite close to each other and show no strong dependence on environmental oxygen partial pressures. However, we suspect that the impurity segregation behavior is quite different for them, and impurity segregation is expected to play more important role in determining the adhesion properties than what is usually expected.

ACKNOWLEDGMENTS

The work is supported by the NSFC (Grants No. 50825205, No. 50821004, No. 50820145203, and No. 10474106), the National 973 Project under Grant No. 2007CB607500, and CAS Project under Grant No. KGCX2-YW-206. W.Z. thanks the SCCAS for time on the Shengteng6800 supercomputer. J.R.S. is supported for this work by the U.S. Office of Naval Research under Grant No. N00014-08-1-1164.

*Corresponding author; wqzhang@mail.sic.ac.cn

[1] *Metal-Ceramic Interfaces*, edited by M. Ruhle, A. G. Evans, M. F. Ashby, and J. R. Hirth (Pergamon, Oxford, 1990).
[2] F. Ernst, Mater. Sci. Eng. R. **14**, 97 (1995).
[3] M. W. Finnis, J. Phys.: Condens. Matter **8**, 5811 (1996).
[4] D. B. Miracle, Acta Metall. Mater. **41**, 649 (1993).
[5] A. Rabiei and A. G. Evans, Acta Mater. **48**, 3963 (2000).
[6] J. Doychak, J. L. Smialek, and T. E. Mitchell, Metall. Mater. Trans. As **20**, 499 (1989).
[7] H. J. Grabke, G. Kurbatov, and H. J. Schmutzler, Oxid. Met. **43**, 97 (1995).
[8] J. C. Yang, E. Schumann, H. Müllejans, and M. Rühle, J. Phys. D **29**, 1716 (1996).
[9] H. J. Grabke, Intermetallics **7**, 1153 (1999).
[10] C. Leyens, B. A. Pint, and I. G. Wright, Surf. Coat. Technol. **133-134**, 15 (2000).
[11] J. A. Haynes, K. L. More, B. A. Pint, I. G. Wright, K. Cooley, and Y. Zhang, Mater. Sci. Forum **369-372**, 679 (2001).
[12] J. A. Haynes, B. A. Pint, K. L. More, I. G. Wright, and Y. Zhang, Oxid. Met. **58**, 513 (2002).
[13] P. Y. Hou and K. Priimak, Oxid. Met. **63**, 113 (2005).
[14] A. Stierle, F. Renner, R. Streitel, and H. Dosch, Phys. Rev. B **64**, 165413 (2001).
[15] A. Stierle, F. Renner, R. Streitel, H. Dosch, W. Drube, and B. C. Cowie, Science **303**, 1652 (2004).
[16] G. Kresse, M. Schmid, E. Napetschnig, M. Shishkin, L. Kohler, and P. Varga, Science **308**, 1440 (2005).
[17] B. Meyer and M. Fähnle, Phys. Rev. B **59**, 6072 (1999), and references therein.
[18] W. Zhang, J. R. Smith, and X. G. Wang, Phys. Rev. B **70**, 024103 (2004), and references therein.
[19] I. G. Batyrev, A. Alavi, and M. W. Finnis, Phys. Rev. B **62**, 4698 (2000).
[20] X. G. Wang, A. Chaka, and M. Scheffler, Phys. Rev. Lett. **84**, 3650 (2000).
[21] W. Zhang and J. R. Smith, Phys. Rev. B **61**, 16883 (2000).
[22] A. Y. Lozovoi, A. Alavi, and M. W. Finnis, Comput. Phys. Commun. **137**, 174 (2001).
[23] J. G. Gay, J. R. Smith, Roy Richter, F. J. Arlinghaus, and R. H. Wagoner, J. Vac. Sci. Technol. A **2**, 931 (1984).
[24] J. C. Boettger, Phys. Rev. B **49**, 16798 (1994).
[25] P. Błoński and A. Kiejna, Surf. Sci. **601**, 123 (2007).
[26] G. Kresse and J. Hafner, Phys. Rev. B **47**, 558 (1993).
[27] G. Kresse and J. Fürthmuller, Phys. Rev. B **54**, 11169 (1996).
[28] G. Kresse and J. Hafner, J. Phys.: Condens. Matter **6**, 8245 (1994).
[29] D. Vanderbilt, Phys. Rev. B **41**, 7892 (1990).
[30] J. P. Perdew, J. A. Chevary, S. H. Vosko, K. A. Jackson, M. R. Pederson, D. J. Singh, and C. Fiolhais, Phys. Rev. B **46**, 6671 (1992).
[31] Ralph W. G. Wyckoff, *Crystal Structures*, 2nd ed. (Interscience, New York, 1964), Vol. 2.
[32] J. W. Feng, W. Q. Zhang, and W. Jiang, Phys. Rev. B **72**, 115423 (2005).
[33] A. Q. Jiang, N. Awasthi, A. N. Kolmogorov, W. Setyawan, A. Borjesson, K. Bolton, A. R. Harutyunyan, and S. Curtarolo, Phys. Rev. B **75**, 205426 (2007).
[34] W. Zhang, J. R. Smith, and A. G. Evans, Acta Mater. **50**, 3803 (2002), and references therein.
[35] R. M. Jaeger, H. Kuhlenbeck, H. J. Freund, M. Wuttig, W. Hoffmann, R. Franchy, and H. Ibach, Surf. Sci. **259**, 235 (1991).
[36] M. Klimenkov, S. Nepijko, H. Kuhlenbeck, and H. J. Freund, Surf. Sci. **385**, 66 (1997).
[37] G. Ceballos, Z. Song, J. I. Pascual, H. P. Rust, H. Conrad, M. Baumer, and H. J. Freund, Chem. Phys. Lett. **359**, 41 (2002).
[38] M. Kulawik, N. Nilius, H. P. Rust, and H. J. Freund, Phys. Rev. Lett. **91**, 256101 (2003).
[39] Y. Lykhach, V. Moroz, and M. Yoshitake, Appl. Surf. Sci. **241**, 250 (2005).
[40] J. R. Smith and W. Zhang, Acta Mater. **48**, 4395 (2000).
[41] D. J. Siegel, L. G. Hector, and J. B. Adams, Surf. Sci. **498**, 321 (2002).
[42] J. Schnitker and D. J. Srolovitz, Modell. Simul. Mater. Sci. Eng. **6**, 153 (1998).
[43] L. A. Bruce and H. Jaeger, Philos. Mag. A **38**, 223 (1978).
[44] J. H. van der Merwe, Philos. Mag. A **45**, 145 (1982).
[45] E. Bauer and J. H. van der Merwe, Phys. Rev. B **33**, 3657 (1986).
[46] A. Vlad, A. Stierle, N. Kasper, H. Dosch, and M. Rühle, J. Mater. Res. **21**, 3047 (2006).
[47] R. X. Hu and P. Nash, J. Mater. Sci. **40**, 1067 (2005).
[48] A. J. Bradley and A. Taylor, Proc. Roy. Soc. London, Ser. A **159**, 56 (1937).
[49] M. W. Chase, C. A. Davies, J. R. Downey, D. J. Frurip, R. A. McDonald, and A. N. Syverud, *JANAF Thermochemical Tables* J. Phys.Chem. Ref. Data Vol. 14, 3rd ed. (American Institute of Physics, New York, 1985).
[50] R. Krachler, H. Ipser, and K. L. Komarek, J. Phys. Chem. Solids **50**, 1127 (1989).
[51] M. Hagen and M. W. Finnis, Philos. Mag. A **77**, 447 (1998).
[52] H. Okamoto, J. Phase Equilib. **14**, 257 (1993).
[53] J. Smialek and I. Glenn, in *Physical Metallurgy*, edited by R. W. Cahn and P. Hassen (Elsevier Science, Amsterdam, 1996), Chap. 14.
[54] J. Libuda, F. Winkelmann, M. Bäumer, H. J. Freund, T. Bertrams, H. Neddermeyer, and K. Muller, Surf. Sci. **318**, 61 (1994).
[55] P. Y. Hou, Annu. Rev. Mater. Res. **38**, 275 (2008).
[56] J. F. Silvain, J. C. Bihr, and J. Douin, Composites, Part A **29**, 1175 (1998).